This is an Author's Original Manuscript (preprint) of an article submitted to 15th IFAC Conference on Programmable Devices and Embedded Systems held in Ostrava, Czech Republic, on 23–25 May 2018. The final version is available online: https://doi.org/10.1016/j.ifacol.2018.07.163.

Simulation of a Gamma Radiation Mapping Using Unmanned Aerial System

Petr Gabrlik * **Tomas Lazna** **

* *Central European Institute of Technology, Brno University of Technology, Brno, Czech Republic (e-mail: petr.gabrlik@ceitec.vutbr.cz)*
** *Central European Institute of Technology, Brno University of Technology, Brno, Czech Republic (e-mail: tomas.lazna@ceitec.vutbr.cz)*

Abstract: This paper investigates the potential of employing unmanned aerial systems (UASs) to gamma radiation mapping and source localisation. Such an approach is advantageous compared to terrestrial radiation mapping, which is, in general, time demanding, and aerial mapping utilising manned vehicles being expensive. The problem mainly stands in the fact that radiation intensity decreases with the square of the distance and thus the UAS should fly as close to the ground as possible. This is often not feasible due to the height differences of terrain and vegetation.
The simulations performed within this contribution examine several scenarios, all of them based on a real mission, where gamma radiation mapping was performed by a terrestrial robot. The results from this experiment are compared with the simulations of UAS-based radiation mapping performed in several flight altitudes and including different source locations. A novel approach, where the flight altitude of UAS varies based on a terrain shape, is also examined and tested on a real data. The results shows, that this technique is highly beneficial, especially in adverse terrain conditions.

Keywords: Gamma radiation, Mapping, Simulation, UAS, Unmanned aerial system, Mobile robots

1. INTRODUCTION

The employing of mobile robotic platforms for ionizing radiation mapping and source localization brings numerous advantages compared to man-involved approaches, but the most evident and substantial one is human health risk minimization. In general, two suitable unmanned platforms for mainland mapping exist: wheel-based terrestrial robots, and unmanned aerial systems (UASs) – flying robots. This paper solely determines the potential of the employing of the UASs in this field.

Terrestrial robots (also unmanned ground vehicles (UGVs)) has been used previously for ionizing radiation mapping (e.g. Jilek (2015), Zakaria et al. (2017)); their main benefit lies in the fact that they operate on the ground level and thus they can localize a radiation source very precisely. On the other hand, UGVs are suitable for small area mapping only due to limited range and operating speed, but the main restriction rests in limited terrain negotiability.

UGVs disadvantages can be compensated by the employing of UASs. Since they operate in free airspace, their operating speed is markedly higher, and the terrain shape and ground obstacles do not affect the operation. However, such an approach has one evident drawback: the radiation intensity decreases with the square of the distance between a source and detector. This difficulty can be suppressed by the utilising of a detector with higher sensitivity, however, such sensors are heavier and the payload capacity of UASs is quite limited. The last option is to operate UAS as close to ground as possible, but there is a risk of collision with terrain and obstacles.

Relevant articles by MacFarlane et al. (2014) and Martin et al. (2015) describe the development and application of light-weight UAS equipped with ionising radiation detector. The unmanned system in the proposed experiment (uranium mines mapping) operates in very low (constant) altitudes above ground level (AGL) of take-off point: 5 and 15 meters in the areas without trees and with trees respectively. Operation in such a low altitudes without the knowledge of terrain shape must be carefully monitored by an operator due to the high risk of collision. Different approach is presented within Sanada and Torii (2015), where an unmanned helicopter was equipped with 6.5 kg sensitive aerial radiation measurement system allowing to measure radiation from altitudes of tens of meters. The proposed measurement near the Fukushima power plant was carried out from an altitude of 80 m. A cooperation between UAV and UGV during radiation search is presented in Christie et al. (2017), another information about

⋆ This work was supported by the European Regional Development Fund under the project Robotics for Industry 4.0 (reg. no. CZ.02.1.01/0.0/0.0/15_003/0000470), and by the grant No. FEKT-S-17-4234 - "Industry 4.0 in automation and cybernetics" financially supported by the Internal science fund of Brno University of Technology.

Fig. 1. Orpheus X-3 UGV (Kocmanova and Zalud (2015)) carrying gamma radiation detectors (left), and DJI S800 UAS equipped with a multi-sensor system for aerial photogrammetry (right).

UAS-based radiation mapping can be found in relevant articles by Kaiser et al. (2017) and Towler et al. (2012).

For the reasons stated above, this work examines the potential of UAS-based radiation mapping from low altitudes, especially in areas with rugged terrain. The common technique, where a UAS operates in a constant altitude, is compared with more advanced approach. The substance of this approach benefits from the knowledge of 3D terrain map allowing to adjust the flight altitude according to the terrain profile. This enables to achieve homogeneous measurements and thus reliable results. Various scenarios, including different flight profiles and source locations and intensities, are investigated utilizing computer simulations.

1.1 Previous work

Our previous research in the field of gamma radiation mapping was mainly focused on a terrestrial robotic mapping. Numerous real experiments have already been carried out (e.g. Jilek (2015)), the most recent one examines the potential of the cooperation between UGV and UAS during such a mapping mission. This experiment, described in detail within Lazna et al. (2018), utilised UAS equipped with a custom-build multi-sensor system (Gabrlik et al. (2018)) for 3D terrain map creation. This map was then used for a trajectory planning for the UGV carrying gamma radiation detectors. The result was very detailed radiation map of a small area where the radiation source was located (Fig. 8), however, a rough radiation map created by the UAS would be beneficial for the initial source localization. Both the UGV and UAS are shown in Fig. 1.

This work is continuation of the above described experiment. The simulations performed herein utilise real data (3D terrain map, source location and intensity, flight trajectory etc.) to determine the results of the UAS-based raditaion mapping.

2. METHODS

This section deals with the theory necessary to perform the simulation first. Then, the exploited equipment is introduced. Finally, the section describes the study area and examined scenarios.

2.1 Theoretical background in the radiation simulation

Multiple effects need to be reflected when modelling the ionizing radiation. Depending on the type of mission, some of them may not be considered. In general terms of the aerial measurement of the radiation, it is meaningful to neglect alpha and beta radiation due to their low penetrability. Moreover, the work is focused on radionuclide sources which leave us only the gamma radiation to deal with.

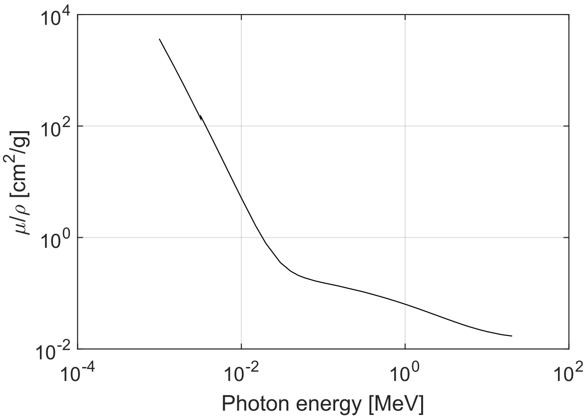

Fig. 2. The dependency of the absorption coefficient on the photon energy.

The intensity of a radionuclide source can be characterized by a dose rate $\dot{D}$ generated by it ($\mathrm{\mu Sv \cdot h^{-1}}$). The dose rate reflects the amount of energy absorbed by a matter; therefore, it depends on the type of the radionuclide as each decays at different energy levels. The dependency is expressed by the exposure rate constant Γ ($\mathrm{R \cdot cm^2 \cdot mCi^{-1} \cdot h^{-1}}$), an overview of its value for different sources can be found in Smith and Stabin (2012). The dose rate also increases with the activity A of the source: a quantity of decays per second (Bq). Given the distance d from the source (m), the dose rate follows the equation (Knoll (2010)):

$$\dot{D} = \frac{\Gamma}{3.7 \cdot 10^5} \frac{A}{d^2}. \quad (1)$$

Another phenomenon that affects the propagation of the radiation is the attenuation. It is characterized by the linear absorption coefficient μ ($\mathrm{m^{-1}}$) which increases with the density and the proton number of the matter and decreases with the increasing energy of the radiation. Given the original intensity I_0, the intensity I in the depth of d is equal to:

$$I = I_0 \cdot e^{-\mu \cdot d}. \quad (2)$$

In technical practice the attenuation is more often expressed by a half-value layer – the thickness of the material at which the intensity is reduced by one half. The absorption coefficient decreases with the increasing energy; the dependency in the air is shown in Fig. 2 (Hubbell and Seltzer (2004)).

The radioactive decay is governed by a statistical law, namely, the Poisson distribution (Campbell and Duarte (2008)). For simplification, let us assume that the number of decays is equal to the number of emitted quanta (photons in case of the gamma radiation). The probability of emission of x photons in one period can be according to the Poisson distribution quantified as:

$$p(x = X) = \frac{e^{-\lambda}\lambda^x}{x!}, \tag{3}$$

where λ states for the mean number of emitted photons per period. Regarding the previous assumptions: $\lambda = A$ for the period of 1 second. The number of emitted photons c in each period is then equal to a random number from the Poisson distribution with the average number of events of λ, denoted as $c \leftarrow \mathcal{P}(\lambda)$.

Ideally, each photon incident to the detector would be registered as one count. However, a real detector has an energy-dependent conversion gain. For a specific pair of a source and a detector, a characteristics may be found in the form of the dependency of the measured counts on the incident dose rate $c = f(\dot{D})$. The characteristics is non-linear mostly due to a phenomenon called the dead time. To take both the statistics and the conversion gain into account, following model is suggested: First, the dose rate generated in one meter $\dot{D}_1$ is calculated for the source and that converted to the number of counts c_1 that would be registered by the corresponding detector. Then, a Poisson random number is picked with the average value equal to the counts c_1. Finally, the inverse square law is included – the number of counts is altered by the square of the distance.

The detector does not register counts induced by the source only, it is affected by a radiation background as well. The natural background has three components: cosmic, terrestrial, and internal; the last one is negligible. The terrestrial radiation is caused by radionuclides occurring in our surroundings in small concentration. The main source is embodied by the uranium and its decay products (thorium, radium, radon, and others). The level of the terrestrial radiation is foremost a function of the geographical location: $\dot{D}_T = f(x, y)$.

The cosmic radiation originates mostly from the nuclear fusion inside stars and explosions (e.g. Supernovae). A major part of it is shielded by the Earth's atmosphere. The cosmic radiation comprises besides photons also other particles such as electrons, neutrinos, and muons which are usually produced by interactions in the upper layers of the atmosphere. The level of cosmic radiation depends especially on the altitude: $\dot{D}_C = f(z)$.

The overall contribution by the background does not follow the Poisson distribution as it consists of multiple independent sources, however, it can be fitted by a Normal distribution. Parameters of the distribution (μ_B, σ_B^2) may be identified empirically within the scope of a single geographic location and for a specific detector.

Total count registered by a detector located at (x_0, y_0, z_0) is composed of counts produced by R sources, each one described by a vector $(\dot{D}_1, x, y, z)$, and of the background counts. Formally, it is expressed by the equation:

$$c = \sum_{i=1}^{R} \frac{[c_1 \leftarrow \mathcal{P}(f(\dot{D}_{1,i}))]e^{-\mu \cdot d_i}}{d_i^2} + c_B \leftarrow \mathcal{N}(\mu_B, \sigma_B^2);$$
$$d_i^2 = (x_i - x_0)^2 + (y_i - y_0)^2 + (z_i - z_0)^2. \tag{4}$$

2.2 Equipment

For the measurement of the gamma radiation, a scintillation detector on the basis of sodium iodide doped with thallium, or NaI(Tl), is employed. The detector has a form of cylindrical two-inch crystal and is encapsulated with a photomultiplier tube. A source of the high voltage for the photodetector as well as signal processing is provided by the multichannel analyzer NuNA MCB3 manufactured by NUVIA. Scintillation detectors are markedly sensitive to the gamma radiation by their nature because of their great volume and density, therefore are suitable for the aerial measurements.

As a radionuclide, the isotope Ceasium-137 (Cs-137) was chosen. Although it is formally a beta source, its decay products emit the gamma radiation at the energy of 662 keV. The absorption coefficient for this energy $\mu = 0.00776 \cdot \rho_A$ where ρ_A is the air's density. Main application of the Cs-137 lies in the field of the radiation therapy, thereby it embodies a rather common source.

The conversion function for the combination of the two-inch NaI(Tl) and the Cs-137 was measured. For dose rates up to 3 μSv $\cdot$ h^{-1}, the dependency is approximately linear with 2200 counts per μSv $\cdot$ h^{-1}.

2.3 Study area

The proposed simulations are situated in real area, near the Brno University of Technology campus (49°13'41.61"N, 16°34'19.002"E — WGS84). The relevant area occupies almost 20,000 m^2 of grassy terrain with large height differences (up to 30 meters), multiple paths, vegetation, and artificial objects. Fig. 3 illustrates the digital elevation model (DEM) of the area created utilising UAS photogrammetry (Gabrlik et al. (2018)).

The coordinates of the model were converted from WGS84 into a local cartesian coordinate system with the origin laying approximately in the centre of the area. All the simulations presented in this paper use this local system.

The background radiation level of the study area was determined using data from available web services and by a measurement. A terrestrial gamma radiation level of 50 nSv $\cdot$ h^{-1} was obtained from the atlas by European Commission (2018), as well as the cosmic radiation level, which is 40 nSv $\cdot$ h^{-1}. The terrestrial radiation was further determined using service Safecast (2018); a value of 110 nSv $\cdot$ h^{-1} approximately correspond with the abovementioned.

The background was also measured using the presented detector in order to determine the number of counts induced by it. The counts were integrated for 30 minutes and then fitted by the Normal distribution resulting in the mean value of 121 CPS and the dispersion of 88 CPS^2.

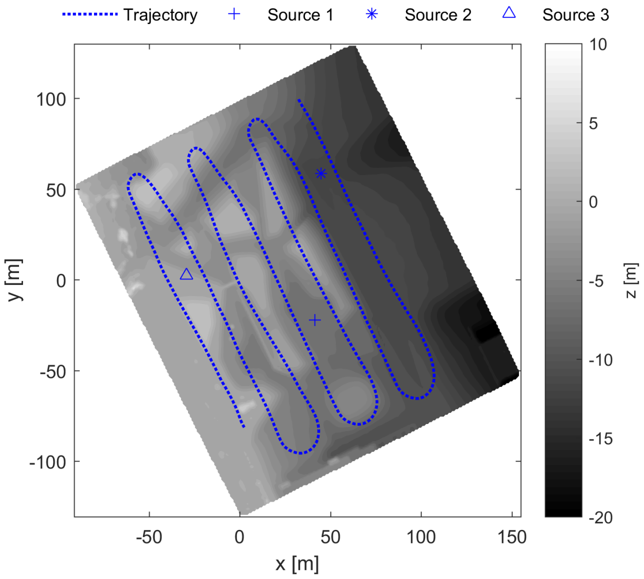

Fig. 3. Digital elevation model of the study area including flight trajectory and source locations. The start location is on the south, end on the north.

2.4 *Simulation scenarios*

The simulation scenarios are based on the experiment introduced in section 1.1. The goal is to examine various combinations of *flight altitudes*, *source locations* and *source intensities*, and evaluate the influence of these parameters on the source localisation.

The original flight trajectory, illustrated in Fig. 3, was left unchanged, except the Z-coordinate – altitude profile. The following three trajectories are included in the simulations:

- *Trajectory 1* – the original X, Y and Z coordinates. The flight altitude was 50 m above start point, which was almost the highest point of the area. The profile was more or less constant, with only small variations.
- *Trajectory 2* – the original X and Y, modified Z coordinate. The flight altitude is constant 10 m above the highest point of the area.
- *Trajectory 3* – the original X and Y, modified Z coordinate. The flight altitude is based on the terrain shape with an offset of 10 m.

The altitude profiles of the flight trajectories, as well as the terrain profile, are illustrated in Fig.4.

Every simulation scenario includes all three flight trajectories; the scenarios differ in the number, location and intensity of gamma radiation sources:

- *Scenario 1* – only the one original Cs-137 source (section 1.1) is present in the area. The source's activity is 35 MBq.
- *Scenario 2* – three identical Cs-137 sources are distributed across the area. The activity of the sources is 35 MBq.
- *Scenario 3* – three identical Cs-137 sources are located on the same places as in the scenario 2. The activity of the sources is ten times higher – 350 MBq.

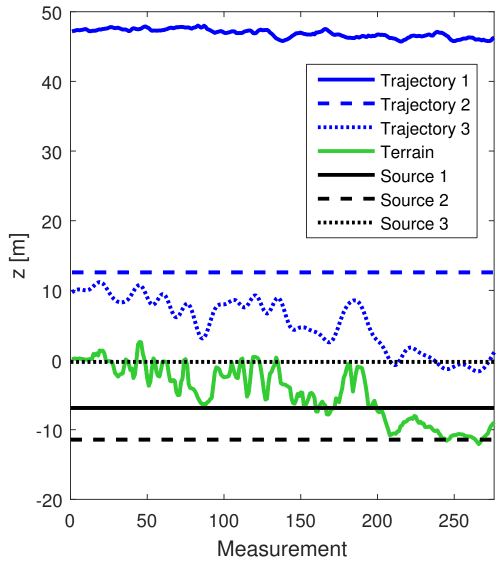

Fig. 4. The profiles of the flight trajectories and the terrain, and the altitude levels of the sources.

The dose rate produced by the weaker sources in 1 m is equal to 3 $\mu\mathrm{Sv} \cdot \mathrm{h}^{-1}$, in case of the stronger sources, the value is 30 $\mu\mathrm{Sv} \cdot \mathrm{h}^{-1}$.

Since three flight trajectories are examined for each of the three scenarios, 9 simulations in total are presented and discussed in the following sections. Fig. 3 and 4 show the sources' locations in XY and Z coordinates respectively.

3. RESULTS

This section presents the results of the simulations performed in MATLAB. Fig. 5, 6 and 7 show the gamma radiation intensity maps as a result of the simulation scenarios 1, 2 and 3 respectively introduced in section 2.4. Each trajectory contains 276 equally distributed positions for whose the radiation intensity was computed. The presented map layers were then created using `contourf` built-in function. The intensity levels are expressed using dimensionless CPS unit; the scales are linear and specific for the individual scenarios. Table 1 further presents the statistic data of the simulations.

Table 1. Statistic data of the simulations.

Scenario #	Traj. #	Min. CPS	Max. CPS	Mean CPS
1	1	99	145	121
1	2	100	144	123
1	3	92	150	123
2	1	94	153	122
2	2	94	149	125
2	3	98	174	129
3	1	105	163	134
3	2	113	363	168
3	3	111	510	189

4. DISCUSSION

A possibility of detecting sources of the gamma radiation using a UAS has been studied within this paper. In the original flight altitude of 50 m which is suitable for the aerial photogrammetry (Gabrlik et al. (2018)), even the strong sources cannot be distinguished from the

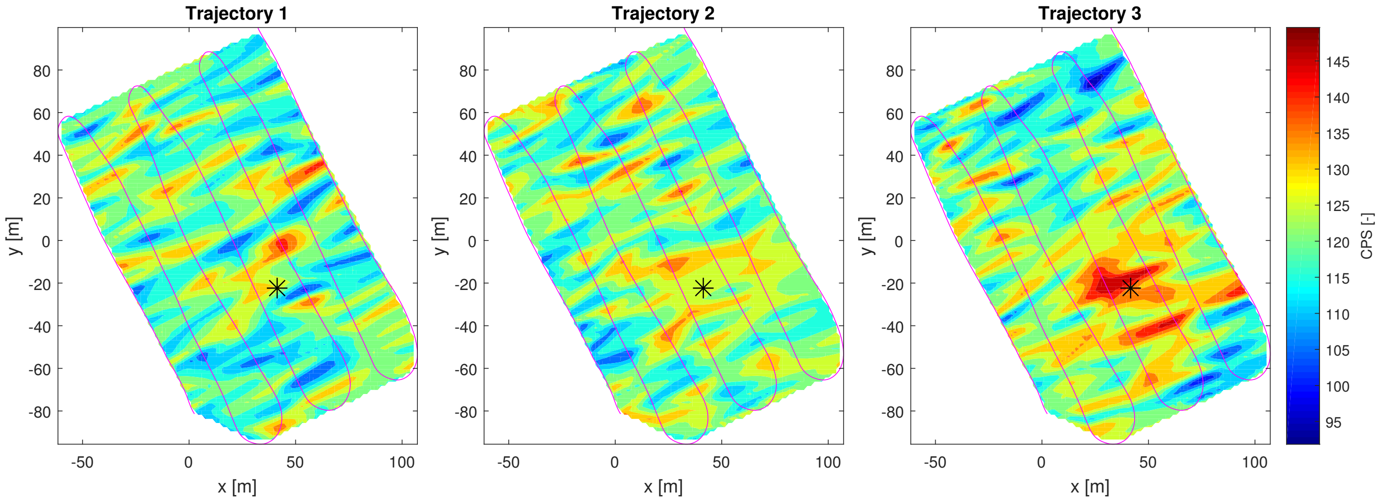

Fig. 5. Radiation intensity maps in the scenario 1 – one 3 μSv · h^{-1} source is present.

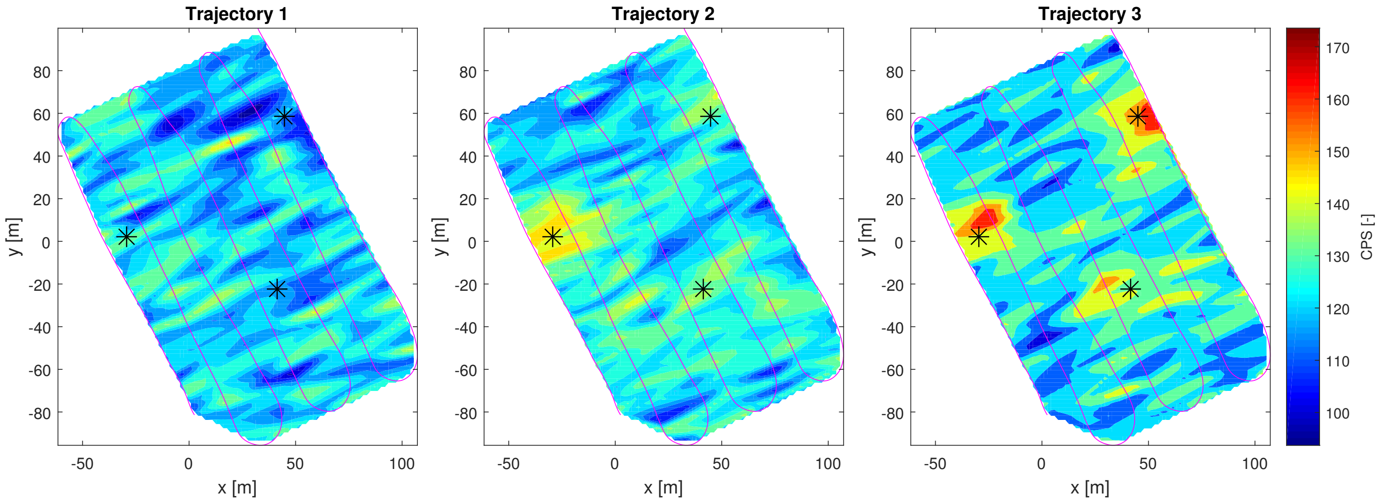

Fig. 6. Radiation intensity maps in the scenario 2 – three 3 μSv · h^{-1} source are present.

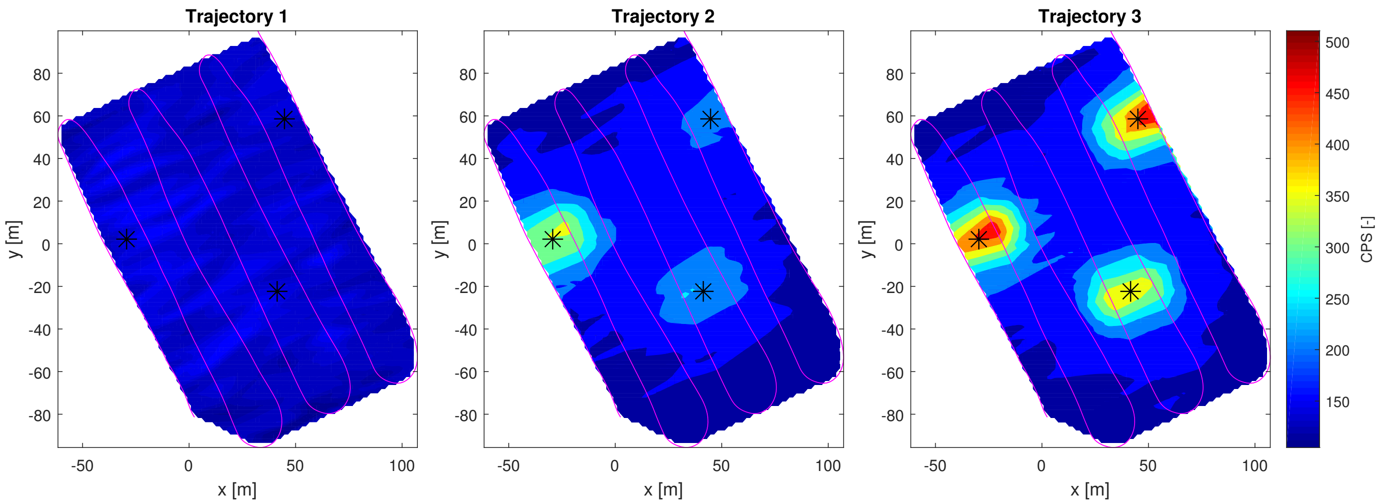

Fig. 7. Radiation intensity maps in the scenario 3 – three 30 μSv · h^{-1} source are present.

background. Such result was expected due to relatively low sensitivity of the employed detector. In the lower flight altitude of 10 m above the highest point of the area, the outcomes start to be meaningful. In the case of the one weaker source (scenario 1), the presence of the source might be judged by eye, however, the statistical significance is insufficient; in other words, the distance from the source along the trajectory is still too great.

When a source is located on a hill (scenario 2), it is detected rather reliably; other two sources are hidden in the background. Regarding the stronger sources (scenario 3), those are fairly distinguishable even in this flight altitude.

The most promising is the approach of the constant altitude above the terrain (trajecotry 3). This method is not dependent on the layout of the sources in an indented environment. In all three scenarios, the sources differ from the radiation background with an adequate statistical significance. The utilization of the method leads to two-phase survey of the area: First, the digital elevation model of the area is acquired. Second, the trajectory for a UAS carrying a radiation detector is planned according to the terrain shape. After the second flight, a preliminary localization of the gamma radiation sources should be available; then it can be followed up by a more precise measurement on the ground level. This approach is evident in Fig. 8, where the radiation map produced by the UAS mapping is compared with the ground mapping performed by a UGV.

The indication of the sources' presence is generally a problem due to the statistical character of the radioactive decay. Each peak in the measured radiation map corresponds either to a source or to a fluctuation in the radiation background. Thus, a prominence of a peak needs to be defined; it should be inferred from a reference level (typically a value in range from the minimal to the mean value) and a prominence level (e.g. a multiple of the standard deviation). The peaks are findable by multiple techniques, for example utilizing Gaussian mixture models (Morelande and Skvortsov (2009)).

A choice of the proper flight altitude depends on two conditions: how strong sources are sought and what prominence above the background is desired. Within this paper, a source producing the dose rate of 3 $\mu\mathrm{Sv} \cdot \mathrm{h}^{-1}$ in 1 meter was considered in the first scenario which corresponds to the Cs-137 with the activity of 35 MBq. Generally, gamma sources with the activity equal or greater than tens of megabequerels are relevant in a context of the radiation protection. For a reliable detection of sources, corresponding peaks should be at least two times higher than the radiation background. In case of the 10^7 Bq sources, that condition would require lower flight altitudes or a more sensitive detector according to the simulations. However, regarding the preliminary aerial survey, less significant peaks approximately 50 % higher than the background can be accepted as well. This condition can already be fulfilled thanks to the suggested copying of the terrain.

A detector with rather low sensitivity was considered in this paper. The reason is that it is light ($\sim$1.3 kg) and still suitable for the type of mission; in addition, the NaI(Tl) is relatively cheap. Applying a more sensitive detector should improve achieved results. One option is to employ a higher volume NaI(Tl) which already proven to be useful. The other option is to choose a plastic detector which has a better ratio of mass-sensitivity. Moreover, it can be manufactured in an arbitrary geometry; it is beneficial for the detector to be more sensitive in the direction to the ground. The key disadvantage is that plastic detectors do not provide spectra, therefore, the

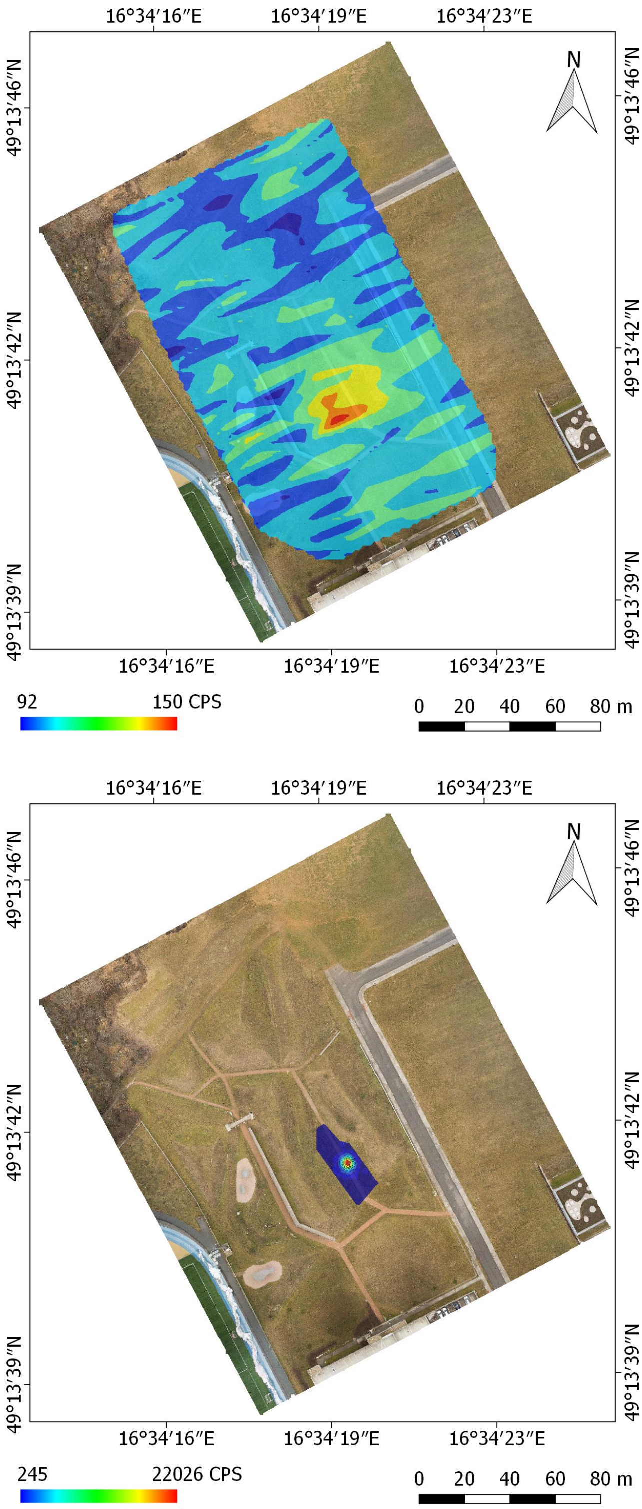

Fig. 8. Radiation intensity layers over an orthophoto map created using UAS photogrammetry. The first one is the result of the UAS radiation mapping simulation (scenario 1, trajectory 3 – section 2.4), and the second one is the radiation layer created by the UGV during the real experiment (section 1.1).

identification of radioisotopes is not feasible. However, if the aerial measurement embodies only the first phase of the mission and is followed by a ground measurement, the lack of spectral information is not an issue.

5. CONCLUSION

This paper examined the potential of lightweight UASs in radiation mapping missions. The evident advantages of the utilising of these systems are fast mapping of large areas, and independence on terrain shape and ground obstacles in general. However, the flight altitude required for a safe operation does not often allow to measure weak radiation sources located on the ground. We investigated multiple scenarios, containing various flight altitudes and source intensities and locations, to determine in which situations are UASs beneficial. Two kind of sources were considered during the simulations: Cs-137 sources with an activity of 35 MBq and 350 Mbq. None of them is detectable from an altitude of 50 m while using 0.1 l scintillation detector, however, 10 m seems to be a sufficient altitude. The problem with the detection occurs at the moment, when the terrain is not flat. For this reason, we proposed a novel approach, where the flight altitude is adjusted according to a terrain profile, which can be obtained from a UAS photogrammetry. The simulations showed, that this method brings more homogeneous and credible results – the sources were detected in all the scenarios. Despite that, the resolution of aerial mapping is not sufficient for precise source localisation in most cases. We suggest to employ UAS for terrain model creation and raw radiation mapping, and then utilise UGV for precise source location within a small region. The comparison of radiation maps produced by the UAS and UGV is also presented at the end of this paper.

REFERENCES

Sara L. Campbell and Javier M. G. Duarte. Poisson Statistics of Radioactive Decay. *MIT Department of Physics*, 2008.

Gordon Christie, Adam Shoemaker, Kevin Kochersberger, Pratap Tokekar, Lance McLean, and Alexander Leonessa. Radiation search operations using scene understanding with autonomous UAV and UGV. *Journal of Field Robotics*, 34(8):1450–1468, November 2017. ISSN 1556-4959. doi: 10.1002/rob.21723.

European Commission. Radiological Maps - European Commission, 2018. URL `https://remap.jrc.ec.europa.eu/Atlas.aspx`. Accessed 2018-03-12.

Petr Gabrlik, Anders la Cour-Harbo, Petra Kalvodova, Ludek Zalud, and Premysl Janata. Calibration and accuracy assessment in a direct georeferencing system for UAS photogrammetry. *International Journal of Remote Sensing*, February 2018. ISSN 0143-1161. doi: 10.1080/01431161.2018.1434331.

J. H. Hubbell and S. M. Seltzer. *X-Ray Mass Attenuation Coefficients*. Physical Measurement Laboratory, National Institute of Standards and Technology, 2004.

Tomas Jilek. Radiation intensity mapping in outdoor environments using a mobile robot with RTK GNSS. In *International Conference on Military Technologies (ICMT) 2015*. IEEE, May 2015. doi: 10.1109/MILTECHS.2015.7153755.

Ralf Kaiser, Iain Darby, Milan Matos, Mladen Bogovac, Richard Murphy, and Phillipe Ortega. UAV-based Mobile Gamma Spectrometry. Vienna, Austria, 2017.

Glenn F. Knoll. *Radiation Detection and Measurement*. John Wiley & Sons, Hoboken, New Jersey, 3rd edition edition, August 2010. ISBN 978-0-470-13148-0.

Petra Kocmanova and Ludek Zalud. Multispectral Stereoscopic Robotic Head Calibration and Evaluation. In *Modelling and Simulation for Autonomous Systems*, Lecture Notes in Computer Science, pages 173–184. Springer, Cham, April 2015. ISBN 978-3-319-22382-7, 978-3-319-22383-4. doi: 10.1007/978-3-319-22383-4_13.

Tomas Lazna, Petr Gabrlik, Tomas Jilek, and Ludek Zalud. Cooperation between an unmanned aerial vehicle and an unmanned ground vehicle in highly accurate localization of gamma radiation hotspots. *International Journal of Advanced Robotic Systems*, 15(1): 1–16, January 2018. ISSN 1729-8814. doi: 10.1177/1729881417750787.

J. W. MacFarlane, O. D. Payton, A. C. Keatley, G. P. T. Scott, H. Pullin, R. A. Crane, M. Smilion, I. Popescu, V. Curlea, and T. B. Scott. Lightweight aerial vehicles for monitoring, assessment and mapping of radiation anomalies. *Journal of Environmental Radioactivity*, 136: 127–130, October 2014. ISSN 0265-931X. doi: 10.1016/j.jenvrad.2014.05.008.

P. G. Martin, O. D. Payton, J. S. Fardoulis, D. A. Richards, and T. B. Scott. The use of unmanned aerial systems for the mapping of legacy uranium mines. *Journal of Environmental Radioactivity*, 143:135–140, May 2015. ISSN 0265-931X. doi: 10.1016/j.jenvrad.2015.02.004.

Mark R. Morelande and Alex Skvortsov. Radiation field estimation using a Gaussian mixture. In *2009 12th International Conference on Information Fusion*, pages 2247–2254, July 2009.

Safecast. Safecast Tile Map, 2018. URL `https://blog.safecast.org/`. Accessed 2018-03-12.

Yukihisa Sanada and Tatsuo Torii. Aerial radiation monitoring around the Fukushima Dai-ichi nuclear power plant using an unmanned helicopter. *Journal of Environmental Radioactivity*, 139:294–299, January 2015. ISSN 0265-931X. doi: 10.1016/j.jenvrad.2014.06.027.

David S. Smith and Michael G. Stabin. Exposure Rate Constants and Lead Shielding Values For Over 1,100 Radionuclides. *Health Physics*, 102(3):271–291, March 2012. ISSN 0017-9078. doi: 10.1097/HP.0b013e318235153a.

Jerry Towler, Bryan Krawiec, and Kevin Kochersberger. Radiation Mapping in Post-Disaster Environments Using an Autonomous Helicopter. *Remote Sensing*, 4(7): 1995–2015, July 2012. doi: 10.3390/rs4071995.

Abd. Hafiz Zakaria, Yasir M. Mustafah, Jaafar Abdullah, Nahrul Khair, and Taufiq Abdullah. Development of Autonomous Radiation Mapping Robot. *Procedia Computer Science*, 105:81–86, January 2017. ISSN 1877-0509. doi: 10.1016/j.procs.2017.01.203.